



## Full Text View

[Volume 28, Issue 3 \(March 1998\)](#)

### Journal of Physical Oceanography

Article: pp. 495–512 | [Abstract](#) | [PDF \(461K\)](#)

# Observations of the Directional Spectrum of Fetch-Limited Waves

**Kevin C. Ewans**

*Shell International Exploration and Production B.V., The Hague, the Netherlands*

(Manuscript received April 17, 1997, in final form July 24, 1997)

DOI: 10.1175/1520-0485(1998)028<0495:OOTDSO>2.0.CO;2

## ABSTRACT

Estimates of the wave directional spectrum of fetch-limited sea states are made from measurements made with a heave–pitch–roll buoy at the Maui location off the west coast of New Zealand. The fetch-limited sea states have significant wave heights between 0.5 and 4.5 m and are observed during persistent southeast wind events, which have a well-defined fetch of 200 km. The integrated properties of the estimated angular spreading distributions are in general agreement with those observed in previous studies. However, the angular distributions estimated for the Maui location are bimodal at frequencies greater than the spectral peak frequency. This result for deep water ocean waves is in contrast to the generally accepted unimodal angular distribution for wind seas, but it supports recently reported measurements of the angular distribution of fetch-limited waves in Lake George, Australia. Parametric relationships that describe the characteristics of the bimodal distributions are derived, and the importance of the bimodality for some applications is discussed.

## 1. Introduction

Many offshore applications require information on the directional characteristics of the wave field. These characteristics can be conveniently specified by the directional wave spectrum. Like the omnidirectional case, our understanding of the nature of the directional wave spectrum is best studied when some of the many variables that contribute to the general sea state are constant. Fetch-limited sea states provide this situation, and the directional distribution of fetch-limited sea states has been the subject of a number of studies. The most significant are those of [Mitsuyasu et al. \(1975\)](#), [Hasselmann et al. \(1980\)](#), and [Donelan et al. \(1985\)](#), each providing parameterizations of a unimodal directional distribution. [Young et al. \(1995\)](#) report an interesting study of fetch-limited waves in Lake George, Australia, where they observed the directional distribution to be bimodal at frequencies greater than twice the spectral peak frequency.

### Table of Contents:

- [Introduction](#)
- [The directional distribution](#)
- [Measurement program and](#)
- [Estimation of the directional](#)
- [Comparison with other](#)
- [The Maui directional](#)
- [Discussion](#)
- [Conclusions](#)
- [REFERENCES](#)
- [FIGURES](#)

### Options:

- [Create Reference](#)
- [Email this Article](#)
- [Add to MyArchive](#)
- [Search AMS Glossary](#)

### Search CrossRef for:

- [Articles Citing This Article](#)

### Search Google Scholar for:

- [Kevin C. Ewans](#)

This paper reports observations of fetch-limited directional spectra, made near to the site of the Maui-A platform off the West Coast of New Zealand (Fig. 1). An earlier study (Ewans and Kibblewhite 1990) showed that at this location southeast winds produce well-defined fetch-limited wind seas at the Maui location. The southeast winds funnel through Cook Strait and the Manawatu Gorge and may persist from just a few hours to several days and sometimes reach gale force. The study showed that the omnidirectional spectrum associated with these “southeast events” conformed closely to the JONSWAP (Hasselmann et al. 1973) spectral shape, and the fetch dependencies of the parameters of the spectrum were quite similar to those observed in the JONSWAP experiment.

Similarly, the southeast winds, which occur approximately 25% of the time at the Maui location, provided a number of well-defined fetch-limited conditions during a subsequent wave directional measurement program. The corresponding sea states, which were measured with a WAVEC heave–pitch–roll buoy are the basis of this paper.

A brief review of the mathematical definitions commonly used to describe the directional distribution and its parameters is given in section 2. The measurement program, data processing, and the procedure for selecting the fetch-limited sea states are described in section 3; the procedures for estimating the directional distributions are given in section 4. Comparisons of the Maui directional distributions with previously published distributions are then given in section 5. This is followed by a description of the particular properties of the Maui distributions and the development of a parameterization, which describes these properties in section 6. A discussion on the importance of the bimodality is given in section 7, followed by the conclusions in section 8.

## 2. The directional distribution

The surface wave field can be described by the two-dimensional frequency–direction spectrum  $S(f, \theta)$ , which is often expressed as the product of the omnidirectional variance density spectrum  $S(f)$ , and the directional distribution  $H(f, \theta)$ , as follows:

$$S(f, \theta) = S(f)H(f, \theta). \quad (2.1)$$

The directional distribution has the properties of a probability density function, namely,

$$H(f, \theta) \geq 0 \quad (2.2)$$

and

$$\int_0^{2\pi} H(f, \theta) d\theta = 1. \quad (2.3)$$

In turn,  $H(f, \theta)$  is often expressed as a Fourier series

$$H(f, \theta) = \frac{1}{\pi} \left\{ \frac{1}{2} + \sum_{n=1}^{\infty} [a_n(f) \cos n\theta + b_n(f) \sin n\theta] \right\}, \quad (2.4)$$

where  $a_n, b_n$  are the Fourier coefficients.

Measures of the central tendency and variation of  $H(f, \theta)$  can be defined in terms of the first ( $n = 1$ ) pair or second ( $n = 2$ ) pair of Fourier coefficients. In terms of the first pair of Fourier coefficients,

$$\theta_1(f) = \arctan \left( \frac{b_1(f)}{a_1(f)} \right) \quad (2.5)$$

and

$$\sigma_1(f) = \{2[1 - (a_1^2(f) + b_1^2(f))^{1/2}]\}^{1/2}. \quad (2.6)$$

Following [Kuik et al. \(1988\)](#),  $\theta_1(f)$  is referred to as the mean wave direction and  $\sigma_1(f)$  the circular rms spreading.

The analogous definitions in terms of the second pair of Fourier coefficients are

$$\theta_2(f) = \frac{1}{2} \arctan\left(\frac{b_2(f)}{a_2(f)}\right) \quad (2.7)$$

and

$$\sigma_2(f) = \left\{ \frac{1}{2} [1 + (a_2^2(f) + b_2^2(f))^{1/2}] \right\}^{1/2}. \quad (2.8)$$

The angle  $\theta_2(f)$  is referred to as the dominant wave direction ([Haring and Heidemann 1980](#)), and the quantity  $\sigma_2(f)$  is referred to as the directional spreading factor ([Forristall and Ewans 1998](#));  $\sigma_2(f)$  corresponds to the square root of the ratio of the variance in line with  $\theta_2(f)$  to the total variance.

### 3. Measurement program and data processing

#### *a. The measurement program*

The wave measurements were made with a Datawell WAVEC buoy moored near the Maui-A platform, 32 km off the west coast of the North Island of New Zealand, in a water depth of 110 m. Measurements commenced in November 1986 and concluded in November 1987. Wind measurements were made with a Lambrecht anemometer installed on the Maui-A platform at a height of 95 m above sea level.

#### *b. Preliminary processing*

The signals of heave and pitch and roll angles were digitized at 1.28 Hz, and on each half hour, coincident and quadrature spectra (co-quad spectra) were computed from the previous 20 minutes of data. Spectral analysis followed the [Welch \(1967\)](#) technique with the final spectrum being an average of six subseries of 200-s length and having approximately 12 degrees of freedom. The co-quad spectra were corrected for the response of the buoy heave filter and then smoothed from 0.16 to 0.50 Hz, resulting in spectra with 0.005-Hz resolution from 0.03 to 0.155 Hz and 0.010-Hz resolution from 0.16 to 0.50 Hz.

The first four Fourier coefficients of the directional spectrum were calculated from the co-quad spectra in the standard way (e.g., [Long 1980](#)), and subsequently spectra for the mean wave direction  $\theta_1(f)$  and the circular rms spreading  $\sigma_1(f)$  were calculated.

The wind data were recorded on a strip chart, from which the 10-min mean speed and direction were obtained at hourly intervals. The wind speeds were reduced to an equivalent wind speed at 10 m above sea level using a neutral wind profile.

#### *c. Selection and processing of steady sea states*

A population of southeasterly spectra was established by selecting all those spectra for which the wind direction was from the southeast and the mean wave direction was within the sector  $100^\circ$ – $150^\circ$ . From this population a subselection of steady spectra was made on the basis that

1. the wind speed was steady to within  $1 \text{ m s}^{-1}$  for at least 4 hours (based on the last five wind estimates), and
2.  $S(f)$ ,  $\sigma_1(f)$ , and  $\theta_1(f)$  were approximately constant for the last 3 hours (based on the last 7 half-hourly spectra).

This selection process resulted in a subpopulation of 77 groups of co-quad spectra, each group containing the half-hourly spectra for the last 3 hours. The co-quad spectra in each group were averaged, resulting in 77 average co-quad spectra for fetch-limited conditions, with each average spectrum having approximately 72 degrees of freedom. The first four Fourier coefficients of the directional spectrum were again calculated from these averages, and in turn spectra for the mean wave

direction  $\theta_1(f)$ , the circular rms spreading  $\sigma_1(f)$ , and the directional spreading factor  $\sigma_2(f)$  were calculated.

A feature of the wave climate at the Maui location is the presence of a more or less persistent swell from the southwest. Fortunately, this component occurs at low-frequency, generally having a peak frequency of around 0.080 Hz ([Ewans and Kibblewhite 1992](#)), is well separated from the wind sea frequency band, and can easily be removed from the analysis by restricting further calculations and analysis to the high-frequency bandwidth corresponding to the local southeast wind sea. In a few cases it was not possible to apply this simple filter because the southeast sea bandwidth extended to low-frequency into the swell band, but these cases corresponded to large local sea states in which the local wind sea component completely swamped the southwest swell component. In these cases, in the frequency region in which the two components overlapped, the spectral levels associated with the wind sea were at least an order of magnitude larger than the swell component, and the mean wave direction at these frequencies was equal to the wind sea mean direction. Even so, results presented later show that the buoy is still able to resolve the directionality of the relatively small swell component in these cases. The selection of the low-frequency cutoff of the wind sea component was done by eye, based on plots of the omnidirectional, mean direction, and circular rms spreading spectra.

A number of parameters were calculated over the band width of the local southeast wind-sea, including the following:

- The maximum  $S(f_p)$  of  $S(f)$  and the frequency of the maximum  $f_p$ .
- The significant wave height,  $H_s = 4(m_0)^{1/2}$ , and the mean wave period,  $T_2 = (m_0/m_2)^{1/2}$ , where the  $m_i$  are the moments of the omnidirectional spectrum.

In addition, the vector average wind speed and direction, averaged over the three hours, were stored for each spectrum.

The 77 spectra had significant wave heights ranging between 0.54 and 4.2 m, mean wave periods between 3.3 and 6.9 s, and had associated vector average wind speeds ranging from 4.6 to 18.3 m s<sup>-1</sup>, and inverse wave ages,  $\bar{u}_{10}/c_p$  [where  $\bar{u}_{10}$  is the 3-h vector average wind speed reduced to 10 m above sea level and  $c_p = g/(2\pi f)$  is the deep water phase speed at the spectral peak], ranging from 0.70 to 1.4.

#### 4. Estimation of the directional distribution

##### a. Model-independent estimates

An estimate was made of the directional distribution from the Fourier coefficients at each frequency, using both the maximum entropy method (MEM) ([Lygre and Krogstad 1986](#)) and the maximum likelihood method (MLM) ([Isobe et al. 1984](#)). Both of these techniques are model independent and allow for the possibility that the distribution may be bimodal.

The resulting MEM and MLM estimates at each frequency were subjected to further analysis, and the following parameters were computed for each:

- The local maxima and minima and their directions. For each estimate there may be either one or two local maxima/minima, depending on whether the particular distribution has respectively one or two peaks.
- Three directional distribution shape parameters as defined by [Kuik et al. \(1988\)](#):  $p$ , the ratio of the area of the distribution from  $\theta_{\max}$  to  $\theta_{\max} - \pi$  to the area of the distribution from  $\theta_{\max}$  (the angle at which the maximum of the distribution occurs) to  $\theta_{\max} + \pi$ ;  $q$ , the ratio of the largest minimum to the smallest maximum (if the distribution is bimodal); and  $r$ , the ratio of the area of the secondary lobe over the area of the main lobe. [Kuik et al. \(1988\)](#) used these parameters to evaluate whether directional distributions could be categorized as unimodal and symmetric or nearly unimodal and symmetric if either a distribution was unimodal but not exactly symmetric or a distribution was strictly bimodal but the secondary lobe was relatively insignificant compared with the main lobe.
- A unimodal/symmetric parameter  $U_{pqr}$ , which is set to 1 if the distribution can be categorized as unimodal and symmetric or nearly unimodal and symmetric (based on the criteria specified in appendix B of [Kuik et al. 1988](#)) and 0 if not.

##### b. Symmetric double Gaussian estimates

An alternative approach to deriving the directional distribution is to assume the true distribution can be described by a parametric model. Several unimodal parametric models that have been proposed are given by [Borgman \(1979\)](#). Included are the “cosine<sup>2s</sup>,” wrapped normal, and von Mises models. An advantage of these models is that the number of parameters needed to describe them is less than four, the number of Fourier coefficients available for calculating them. The disadvantage of unimodal distributions is that they cannot describe the directional distribution at a given frequency in which wave components are arriving from different directions.

Bimodal distributions can, of course, describe up to two components, but in general they require more than four parameters to describe them. While four-parameter bimodal models have been proposed, by [Hasselmann et al. \(1980\)](#) and [Borgman and Yfantis \(1978\)](#), they are not ideal. The bimodal model proposed by Hasselmann et al. is a double cosine model in which both spreading parameters are forced to be equal to obtain a unique solution, and in the case of the Borgman and Yfantis model, the parameters cannot be directly related to the properties of the wave field.

More recently, [Benoit \(1993\)](#) describes an evaluation of a bimodal Gaussian model containing five parameters, which are calculated from the co–quad spectra by a least squares method. Benoit concluded that the method gave good estimates, but the evaluations were based on simulations of measurement arrays with at least four elements. A heave–pitch–roll buoy is effectively a three-element array, for which Benoit’s bimodal Gaussian model contains too many parameters.

The properties of the MEM and MLM directional distributions of the Maui fetch-limited sea states presented in [section 6b](#), suggest that the number of parameters in the bimodal Gaussian model can be reduced for fetch-limited sea states. In particular, it is reasonable to assume that the directional distribution is symmetric about the mean, and therefore that each of the two components of the bimodal Gaussian distribution can be assumed to have both the same amplitude and the same spreading. The proposed bimodal distribution then has the following form:

$$\begin{aligned}
 H(f, \theta) &= \frac{1}{\sqrt{8\pi}\sigma(f)} \sum_{k=-\infty}^{\infty} \left\{ \exp\left[-\frac{1}{2}\left(\frac{\theta - \theta_{m1}(f) - 2\pi k}{\sigma(f)}\right)^2\right] \right. \\
 &\quad \left. + \exp\left[-\frac{1}{2}\left(\frac{\theta - \theta_{m2}(f) - 2\pi k}{\sigma(f)}\right)^2\right] \right\}, \tag{4.1}
 \end{aligned}$$

where  $\sigma(f)$  is the angular width and is a measure of the spreading of each component and  $\theta_{m1}(f)$  and  $\theta_{m2}(f)$  are the locations of the peaks.

The Fourier coefficients for this function are given by

$$\begin{aligned}
 a_1 &= \exp\left(\frac{-\sigma^2}{2}\right) \cos(\theta_{m1}) + \exp\left(\frac{-\sigma^2}{2}\right) \cos(\theta_{m2}) \\
 b_1 &= \exp\left(\frac{-\sigma^2}{2}\right) \sin(\theta_{m1}) + \exp\left(\frac{-\sigma^2}{2}\right) \sin(\theta_{m2}) \\
 a_2 &= \exp(-2\sigma^2) \cos(2\theta_{m1}) + \exp(-2\sigma^2) \cos(2\theta_{m2}) \\
 b_2 &= \exp(-2\sigma^2) \sin(2\theta_{m1}) + \exp(-2\sigma^2) \sin(2\theta_{m2}). \tag{4.2}
 \end{aligned}$$

[Equation \(4.2\)](#) is a set of four equations with three unknowns,  $\sigma$ ,  $\theta_{m1}$ , and  $\theta_{m2}$ , which can be solved by a least square approach. The objective function  $O$  to be minimized is

$$O = (\hat{a}_1 - a_1)^2 + (\hat{b}_1 - b_1)^2 + (\hat{a}_2 - a_2)^2 + (\hat{b}_2 - b_2)^2, \tag{4.3}$$

where, for example,  $\hat{a}_1$  is the first Fourier coefficient, estimated from the data.

[Equation \(4.3\)](#) was solved for each frequency of the 77 spectra by a nonlinear optimization with the constraints that  $0 \leq \sigma(f), \theta_{m1}, \theta_{m2} \leq 2\pi$ . Initial guesses of the three parameters were obtained from the MEM estimates. The results are presented in [section 6c](#).

## 5. Comparison with other distributions

### a. Mitsuyasu distribution

[Mitsuyasu et al. \(1975\)](#) measured directional wave spectra with a cloverleaf buoy, at open sea locations in the Sea of Japan and the Pacific Ocean and in a bay on the east coast of Japan. Meteorological data were collected from a tending ship near each observation station. They chose five datasets for estimating the directional distribution, with wind speeds ranging from 7 to 10 m s<sup>-1</sup> and significant wave heights from 0.74 to 2.34 m. The cloverleaf buoy enables the first four pairs of the coefficients in [Eq. \(2.4\)](#) to be calculated. However, the higher-order coefficients, which are available from the measurement of the wave curvature, were not used because they were thought to be inaccurate. Thus, the data used by [Mitsuyasu et al. \(1975\)](#) were the same as if the measurement instrument was a heave-pitch-roll buoy.

The Mitsuyasu distribution is based on the “cosine2s” form,

$$H(f, \theta) = A(s) \cos^{2s} \left( \frac{\theta - \theta_1(f)}{2} \right), \quad (5.1)$$

where  $A(s)$  is a normalization factor to ensure [Eq. \(2.3\)](#) is satisfied. The parameter  $s$  is a function of frequency.

Based on their data, [Mitsuyasu et al. \(1975\)](#) proposed the following parameterization for  $s$ :

$$s = \begin{cases} s_p \left( \frac{f}{f_p} \right)^5, & f < f_p \\ s_p \left( \frac{f}{f_p} \right)^{-2.5}, & f \geq f_p, \end{cases} \quad (5.2)$$

where  $s_p$  is the value of  $s$  at the frequency of the spectral peak  $f_p$ , given by

$$s_p = 11.5 \left( \frac{u_{10}}{c_p} \right)^{-2.5}, \quad (5.3)$$

where  $u_{10}$  is the wind speed at 10 m MSL. The directional distribution defined by [Eqs. \(5.1\), \(5.2\), and \(5.3\)](#) will be referred to as the Mitsuyasu distribution in the remainder of this paper.

### b. Hasselmann distribution

[Hasselmann et al. \(1980\)](#) report an analysis of data recorded during the JONSWAP experiment. The directional wave data were collected with a heave-pitch-roll buoy located in 22 m of water 52 km off the island of Sylt in the North Sea. Meteorological data were also collected at this site and a meteorological buoy located 27 km offshore in a water depth of 18 m. The dataset chosen for analysis ranged in wind speed from 6.8 to 15.0 m s<sup>-1</sup> and significant wave heights from 0.55 to 1.88 m.

The parameterization proposed by [Hasselmann et al. \(1980\)](#) for their directional distributions is also based on the cosine2s form with the following parameterization for  $s$ :



$$s = \begin{cases} 9.77 \left( \frac{f}{f_p} \right)^\mu, & f \geq 1.05 f_p, \end{cases} \quad (5.4)$$

where  $\mu$  has a dependence on wave age as follows:

$$\mu = -2.33 - 1.45 \left( \frac{u_{10}}{c_p} - 1.17 \right). \quad (5.5)$$

The directional distribution defined by [Eqs. \(5.1\)](#), [\(5.4\)](#), and [\(5.5\)](#) will be referred to as the Hasselmann distribution in the remainder of this paper.

### c. Donelan distribution

[Donelan et al. \(1985\)](#) report an analysis of data recorded with an array of 14 wave staffs in Lake Ontario and a similar, scaled down version in a large laboratory tank. The wave staffs were mounted on a tower 1 km offshore in a water depth of 12 m. Meteorological data were also collected from the tower and with a buoy 11 km from the tower in deeper water. Eighty-five field recordings and seven laboratory recordings were used in the analysis. [Donelan et al. \(1985\)](#) do not report the absolute range of wind speed and significant wave heights associated with their analysis dataset, but the field data were in the range  $0.83 < u_{10}/c_p < 4.6$  and the laboratory data in the range  $7.2 < u_{10}/c_p < 16.5$ .

Based on the theoretical directional characteristics of freely propagating, second-order Stokes wave groups and analysis of their data, [Donelan et al. \(1985\)](#) proposed the following directional distribution:

$$H(f, \theta) = 0.5\beta \operatorname{sech}^2\beta(\theta - \theta_1(f)), \quad (5.6)$$

where

$$\beta = \begin{cases} 2.61 \left( \frac{f}{f_p} \right)^{1.3}, & 0.56 < f/f_p < 0.95 \\ 2.28 \left( \frac{f}{f_p} \right)^{-1.3}, & 0.95 < f/f_p < 1.6 \\ 1.24, & f/f_p > 1.6. \end{cases} \quad (5.7)$$

The [Donelan et al. \(1985\)](#) dataset only extended to  $f/f_p = 1.6$ . Thus, the constant value of  $\beta = 1.24$  for frequencies greater than 1.6 was assumed.

The directional distribution defined by [Eqs. \(5.6\)](#) and [\(5.7\)](#) will be referred to as the Donelan distribution in the remainder of this paper.

### d. Donelan–Banner distribution

Based on high-frequency stereo photography, [Banner \(1990\)](#) concluded that  $\beta$  was not a constant at values of  $f/f_p > 1.6$  as specified by [Donelan et al. \(1985\)](#) and proposed that

$$\beta = 10^{\{-0.4 + 0.8393 \exp[-0.567 \ln(f/f_p)^2]\}}, \quad f/f_p > 1.6. \quad (5.8)$$

Thus, this distribution, referred to as the Donelan–Banner distribution in this paper, consists of the Donelan distribution but with the Banner value for  $\beta$  for  $f/f_p > 1.6$ .

### e. Comparisons with the Maui data

## 1) THE $s$ PARAMETER

The  $s$  parameter in the cosine $^2s$  distribution can be estimated directly from the circular rms spreading as

$$s = \frac{2}{\sigma_1^2} - 1. \quad (5.9)$$

This parameter was calculated for all 77 Maui spectra and is plotted as a function of  $f/f_p$  in [Fig. 2](#). Also plotted in [Fig. 2](#) are the  $s$  values from the Mitsuyasu and the Hasselmann distributions for  $u_{10}/c_p = 0.7$  and 1.4. [Figure 2](#) shows that the Maui data are in general agreement with previous observations of this parameter—the spreading is a minimum ( $s$  maximum) at the spectral peak but increases with increasing and decreasing frequency. With the exception of the Mitsuyasu  $u_{10}/c_p = 0.7$  distribution, the Maui distributions, with higher  $s$  values, show less directional spreading than the other distributions in the region of  $f_p$  and over the high-frequency range of the spectrum. The data also show a more rapid increase in spreading with decreasing frequency below  $f_p$ .

[Hasselmann et al. \(1980\)](#) argue that, if the directional spreading is controlled predominantly by nonlinear wave–wave interactions, then  $s$  should depend mainly on  $f/f_p$  while, if atmospheric input was the controlling process, then  $s$  should depend mainly on  $u_{10}/c_p$ . To investigate the behavior of the Maui  $s$  values, the spectra were categorized into groups of inverse wave age, the frequency normalized by  $f_p$  and binned, and an average  $s$  value calculated for each bin. This resulted in average  $s$  curves for each category, and these are plotted in [Fig. 3](#).

The curves in [Fig. 3](#) are essentially superimposed under the frequency normalization. There is, however, some indication of a small systematic difference between the curves over the frequency range  $1.5 < f/f_p < 3$  and, hence, a possible weak dependence of  $s$  on  $u_{10}/c_p$ .

For direct comparison with the Mitsuyasu and Hasselmann functions a parameterization for  $s$  was established for the Maui data. Following the same approach as [Mitsuyasu et al. \(1975\)](#) and [Hasselmann et al. \(1980\)](#), it was assumed that  $s$  could be determined by a relation of the form

$$s = k \left( \frac{f}{f_p} \right)^m \quad (5.10)$$

and the constants  $k$  and  $m$  determined by linear regression analysis of  $\log(s)$  versus  $\log(f/f_p)$ .

The linear regression was performed on the data for  $f/f_p < 1$  and for  $f/f_p \geq 1$ . On the basis of the lack of a clear dependence of the Maui  $s$  parameter on  $u_{10}/c_p$ , all 77 spectra were included in the regression.

The analysis resulted in the following  $s$  parameterization for the Maui data:

$$s = \begin{cases} 15.5 \left( \frac{f}{f_p} \right)^{9.47}, & f/f_p < 1 \\ 13.1 \left( \frac{f}{f_p} \right)^{-1.94}, & f/f_p \geq 1. \end{cases} \quad (5.11)$$

## 2) THE $\Sigma_1$ PARAMETER

[Figure 4](#) gives a comparison of the circular rms spreading calculated from the Maui data with the published distributions. The Mitsuyasu and Hasselmann curves have been included by applying [Eq. \(5.9\)](#); while the Donelan and Donelan–Banner curves have been determined from [Eq. \(2.6\)](#), where the Fourier coefficients were derived from the respective distributions. Again, good general agreement is seen between the Maui and other distributions, but at the peak frequency the Maui  $\sigma_1$  values are closer to the Donelan and Donelan–Banner distributions than to the Mitsuyasu ( $u_{10}/c_p =$



1.4) and Hasselmann distributions (both of which suggest more spreading in the region of the peak). The Mitsuyasu ( $u_{10}/c_p = 0.7$ ) curve shows the least spreading in the region of the peak. At higher frequencies,  $f/f_p > 1.4$ , it is clear that the spreading is not constant as given by the Donelan distribution.

When the Maui  $\sigma_1$  data are grouped into the same wave age categories as the  $s$  data presented in [Fig. 3](#), no significant wave age dependency is apparent ([Fig. 5](#)); although as for the  $s$  parameter curves in [Fig. 3](#), a small systematic difference between the [Fig. 5](#) curves over the frequency range  $1.5 < f/f_p < 3$  indicates the possibility that a weak dependency may exist.

### 3) THE $\Sigma_2$ PARAMETER

A comparison of the directional spreading factor calculated from the Maui data with the published distributions is given in [Fig. 6](#). The curves have been determined from [Eq. \(2.8\)](#), where the Fourier coefficients are derived from the respective distributions. Again there is good qualitative agreement between the Maui data and the published distributions. The directional spreading factor attains a maximum at the peak frequency and decreases with increasing and decreasing frequency. At around  $f/f_p = 2.8$  the Maui  $\sigma_2$  values tend to a minimum, but at higher frequencies they increase again. The increase of  $\sigma_2$  above  $f/f_p = 2.8$  results from an increase in the in-line variance that occurs at these frequencies.

It is clear from the figure that the Maui  $\sigma_2$  values are significantly higher than the Hasselmann and Mitsuyasu ( $u_{10}/c_p = 1.4$ ) curves in the region of the peak frequency, and over most of the frequency range they are more or less bounded by the Donelan–Banner and the Mitsuyasu ( $u_{10}/c_p = 0.7$ ) curves.

As for the  $\sigma_1$  data, the  $\sigma_2$  values grouped by wave age, presented in [Fig. 7](#), show some but inconclusive evidence for a weak dependence on wave age for  $f/f_p > 1.5$ .

## 6. The Maui directional distribution

### a. Characteristics of the MEM and MLM distributions

The cosine $2s$  parameterization of the Maui data derived in [section 5e\(1\)](#) permits a directional distribution function to be ascribed to the Maui fetch-limited data, which is unimodal, symmetric but based only on the first pair of Fourier coefficients in [Eq. \(2.4\)](#). The estimates of the directional distribution, using the maximum entropy and maximum likelihood methods, make use of all of the Fourier coefficients available from heave–pitch–roll buoy data. The resulting distributions show that a simple cosine $2s$  form is not appropriate for the fetch-limited Maui data. In particular, the estimates show that for frequencies above the spectral peak a unimodal, symmetric distribution is not appropriate.

[Figure 8](#) is an example of the MEM and MLM estimates for one of the spectra ( $H_s = 3.8$  m,  $T_2 = 6.4$  s), and [Fig. 9](#) shows frequency slices through these spectra. Both distributions are unimodal at the peak frequency but become bimodal at frequencies above the spectral peak, with the MEM estimate becoming bimodal at around 0.17 Hz ( $\sim 1.4f_p$ ) and the MLM at around 0.25 Hz ( $\sim 2f_p$ ).

The observation that fetch-limited sea states have bimodal distributions at frequencies greater than the spectral peak frequency has previously been reported by [Young et al. \(1995\)](#), who showed that their directional spectra, which were recorded with a wave gauge array, demonstrated bimodality at frequencies greater than  $2f_p$ . This provided experimental confirmation of earlier work by [Banner and Young \(1994\)](#), who showed that the directional distribution of components in the equilibrium range of the spectrum were bimodal when calculations were made using the full solution to the nonlinear wave–wave interaction source term. [Young et al. \(1995\)](#) presented a comparison between a directional spectrum calculated this way with their spectra and showed that there was good agreement. Accordingly, they concluded that the bimodal effect they observed was caused by nonlinear wave–wave interactions. They also speculated why the phenomenon had not been previously reported and cited a number of publications in which the effect was visible but apparently given little or no attention. They also made the observation that the effect will clearly not be observed in studies based on analyses where the directional distribution has been assumed to be unimodal, such as reported by [Mitsuyasu et al. \(1975\)](#).

The [Young et al. \(1995\)](#) data were collected with a wave gauge array in Lake George, Australia. The lake had a water depth of 2 m and the reported waves were in the range  $1.7 < u_{10}/c_p < 3$ . The Maui spectra show that the effect is also present in open ocean conditions. In addition as the effect has been observed with a heave–pitch–roll buoy, it can be

concluded that a three-element system, which provides estimates of the first two pairs of Fourier coefficients in Eq. (2.4), is capable of resolving the bimodality.

A feature of the estimates was that the MEM estimate always gave an apparent improvement in the resolution of the bimodal effect. Previous studies (e.g., [Nwogu et al. 1987](#)) have noted the high resolving power of the MEM estimate by comparison with the MLM estimate, while others (e.g., [Brisette and Tsanis 1994](#)), based on synthetic data, have concluded that the MEM estimate may at times provide two peaks when there is actually only one. [Krogstad \(1991\)](#) argues that this observation is not necessarily a weakness of the MEM estimate on the grounds that, if the form of the directional distribution is already known, then additional information is known and the MEM estimate is no longer an optimal estimate. While such a result has not been reported for the MLM estimates, it has been observed to artificially broaden the spectrum ([Young 1994](#)). Of course, when we are estimating directional spectra from data measured in the open ocean, we do not know the directional distribution a priori and therefore we cannot dismiss either of the estimates. However, it should be noted that the MEM estimate preserves the Fourier coefficients—that is, the Fourier coefficients calculated from the estimate are identical to those used to estimate it; this is not the case for the MLM estimate. In view of these issues, both MEM and MLM estimates were made from the Maui data, and both sets investigated in parallel.

The extent of the bimodality in the MEM and MLM estimates was compared by estimating the percentage of unimodal/symmetric estimates, as given by the unimodal/symmetric parameter  $U_{pqr}$ . This is plotted as a function of  $f/f_p$  in [Fig. 10](#). The figure shows that in the region of the peak frequency both estimates produce predominantly unimodal/symmetric distributions. However, while this occurs through to around  $f/f_p \sim 1.7$  in the case of MLM, the percentage of MEM unimodal/symmetric distributions quickly diminishes with increasing  $f/f_p$ , and there are effectively no occurrences above  $f/f_p \sim 1.7$ . The percentage of MLM unimodal/symmetric distributions also decreases above  $f/f_p \sim 1.7$ , but increases again above  $f/f_p \sim 3$ . It is not clear why this tendency occurs but, whenever the distribution is unimodal/symmetric at  $f/f_p > 3$ , the peak is located at an angle close to that of one of the peaks of a neighboring bimodal distribution. The figure also indicates occurrences of distributions that are not unimodal/symmetric below  $f/f_p = 1.0$  for both MEM and MLM distribution types, indicating the existence of bimodal distributions at frequencies below the peak, something which was noted by [Young et al. \(1995\)](#) to occur in the theoretical estimate of the directional spectrum. However, the increase in the number of bimodal distributions below  $f/f_p = 1.0$  in the Maui data may result from the presence of a swell component in some of the spectra.

### *b. Characteristics of the components of the MEM and MLM distributions*

The results presented in the previous section clearly indicate that at frequencies sufficiently greater than the peak frequency a bimodal representation of the directional distribution is more appropriate than a unimodal one; they also indicate that this may be the case at frequencies less than the peak frequency. This suggests that fetch-limited sea states have bimodal directional distributions.

An ideal fetch-limited event will have a directional distribution symmetric about the mean direction; and, if that distribution is indeed bimodal, the two modes will be identical. It is therefore of interest to assess the degree of symmetry that exists in the Maui distributions. This can be done by comparing the properties of the two peaks or components identified in the MEM and MLM estimates.

In order to quantify the properties of the components that make up the MEM and MLM distributions, the estimates were peak fitted with a pseudo-Voigt function. The pseudo-Voigt function is a combination of a Gaussian and Lorentzian (or Cauchy) distribution. The combination allows for a flexible fit to a peak—the Lorentzian distribution allowing for a broad distribution and the Gaussian distribution accommodating a peaked distribution. Thus, an equation of the following form (the pseudo-Voigt function) was fitted to each distribution:

$$H(f, \theta) = \sum_{i=1}^n A_i(f) [F_i(f)L(\theta) + (1 - F_i(f))G(\theta)], \quad (6.1)$$

where

$$G(\theta) = \sum_{k=-5}^5 \exp \left[ -2.77 \left( \frac{\theta - \theta_i(f) - 2k\pi}{\Gamma_i(f)} \right)^2 \right] \quad (6.2)$$

and

$$L(\theta) = \sum_{k=-5}^5 \frac{\Gamma_i^2(f)}{4(\theta - \theta_i(f) - 2k\pi)^2 + \Gamma_i^2(f)}. \quad (6.3)$$

The values of the parameters of the  $i$ th peak— $A_i(f)$  the amplitude,  $F_i(f)$  the fraction of Lorentzian to Gaussian function,  $\theta_i(f)$  the direction, and  $\Gamma_i(f)$  the half-width (or the full width at half height)—quantify the components.

The summation in [Eq. \(6.1\)](#) allows for the possibility of one ( $n = 1$ ) or two peaks ( $n = 2$ ) in the spectrum, and the summation over  $k$  in the Gaussian and Lorentzian functions ensures the distributions are wrapped over  $2\pi$  (the range from  $-5$  to  $5$  was found to be sufficient to give a good fit to all the estimates).

Plots of the locations of the peaks of the two component ( $n = 2$ ) fits to the MEM distributions and of their angular separation are given in [Fig. 11](#). When plotted in this way the angular separation for each spectrum essentially collapse onto a single curve, indicating that the angular separation can be considered a function of  $f/f_p$  only. The continuous lines are the locations of the maxima and their angular separation [respectively plots (a) and (b)] of the Exact-NL distribution presented in [Young et al. \(1995\)](#). It should be noted here that the Exact-NL lines are derived from the maxima of the Exact-NL distribution, whereas the Maui points are the maxima of the component peaks. The locations of the maxima of the Exact-NL distribution components, which would be directly comparable with the Maui points, are likely to be slightly different (larger separation) to those given by the lines. This difference will be small at higher frequencies where the peaks are well resolved but larger at lower frequencies where the components of the distribution begin to merge.



The data were also categorized into groups of inverse wave age, binned into  $f/f_p$  classes, and an average angular separation calculated for each bin. The resulting average angular separation curves for each category are plotted in [Fig. 12](#). As was found for the other parameters where this type of plot was produced, there is no clear dependence of angular separation on wave age, but over the frequency range  $1.5 < f/f_p < 3$ , the angular separation tends to be larger for higher values of  $u/c_p$  or equivalently for the “younger” wind seas. Thus, some weak dependence of the angular separation on wave age cannot be entirely discounted over this range of  $f/f_p$ .



[Figures 11](#) and [12](#) show clearly that the Maui distributions are bimodal above the peak frequency. They also indicate bimodality for frequencies below the peak frequency, but the spread of some of these locations around the southwest and west directions suggest that a number of these points are small swell components. In the analysis, the low-frequency swell was excluded from further analysis (by excluding the frequency band of the swell) except where the wind sea component extended into low frequencies and “swamped” the swell component. The figures show that the buoy and analysis is still able to resolve the small swell component in these cases.


The Phillips turbulent pressure fluctuation theory for wave growth also predicts a bimodal wave direction spectrum. The theory predicts that wave growth is largest when the component of wind velocity in the direction of propagation equals the wave speed. A “resonance” angle  $\Phi = \sec^{-1}(U/c)$  is defined ([Longuet-Higgins et al. 1963](#)). The expected angular separation of peaks based on  $\Phi$  calculated from the Maui data (wind and phase speeds) are plotted in [Fig. 12](#). Clearly, these resonance angle peak separation values do not match the observed Maui curves. This result, together with the fact that the resonance angle is only a function of wave age, whereas no clear dependency of any of the directional parameters on wave age could be identified in the Maui data, suggests that the Phillips turbulent pressure fluctuation theory for wave growth is not responsible for the observed angular separation. On the other hand, the Exact-NL lines on the plots ([Fig. 11](#)) show remarkably good agreement with the Maui data, leading to the conclusion that it is nonlinear wave-wave interactions that are primarily responsible for the bimodality.

The properties of the two components were examined by categorizing them as either right or left, depending on whether a clockwise or an anticlockwise rotation is required to rotate from the mean direction to the direction of the component’s peak. These are plotted in [Fig. 13](#). [Figure 13a](#) is a plot of the right and left peak location relative to the mean  $\theta_1$  at that frequency, [Fig. 13b](#) is a plot of the respective amplitudes, and [Fig. 13c](#) is that of the half-widths. In the plots, points with  $f/f_p < 1.3$  are plotted as open circles.

If the right and left properties were equal, all the points would lie on the straight line. If all points of all the properties lay on the straight line, then the distribution would be perfectly symmetrical. This is clearly not the case, but in general, it can be seen that it is mostly the higher amplitude ([Fig. 3b](#)) points with  $f/f_p < 1.3$  that are farthest from the straight line—the points with  $f/f_p \geq 1.3$  more or less lie on the straight line.

Many of the total number of distributions with frequencies in the region of the spectral peak were unimodal and symmetric (see [Fig. 10](#) ); those that were not (plotted in [Fig. 13](#) ) were often nearly unimodal, in which the distribution comprised one large peak and a secondary smaller one that accounted for a small sidelobe to the main peak. These cases account for the majority of the distributions that are not symmetric.

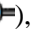
Nevertheless, the asymmetry that is evident to a larger or smaller extent at all frequencies in [Fig. 13](#)  should not be overlooked. For  $f/f_p < 1.3$ , the right amplitude is often substantially larger than the left one and closer to the mean direction; this is consistent with a nearly unimodal distribution. For  $f/f_p \geq 1.3$ , the points in [Figs. 13a and 13b](#)  appear to follow a straight line with a slope slightly different from unity. It is not clear what is responsible for the apparent asymmetry; but possible causes might be some residual effect of the low-frequency swell or some asymmetry in the fetch, which would account for the increased asymmetry in the low-frequency, older, components and the reduction in the asymmetry at higher frequencies (larger  $f/f_p$ ). The measured directional distributions reported by [Young et al. \(1995\)](#) also show some asymmetry, but they believed this to be due to sampling variability—something that is also present in the Maui data.





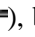

Comparable plots to those in [Figs. 11–13](#) , made for the MLM data but not given here, showed similar effects. The more significant differences were that the MLM plots had fewer points (i.e., fewer bimodal distributions in the MLM), the angular separation was slightly smaller, and the half-widths slightly larger than the MEM distribution points.

### *c. A proposed parameterization based on the symmetric double Gaussian distribution*

In this section, a new parameterization is developed for the directional distribution of fetch-limited sea states. The parameterization defines the bimodality for frequencies above the spectral peak, while maintaining consistency with the integrated spreading parameters  $\sigma_1$  and  $\sigma_2$ .

Based on the characteristics demonstrated in the previous section it is assumed that the bimodality displayed by the distributions above the peak is symmetric. This is supported by the heuristic argument that, if the bimodality is a robust feature of nonlinear wave–wave interactions, the growth of each peak should be equal.

In addition, while the general shape of the MEM and MLM estimates are similar, it is clear that their differences (e.g., see [Fig. 9](#) ) which arise because of the limited number of available Fourier coefficients, suggest that there is a number of possible functions that will give the same first four Fourier coefficients of the measured distribution. For convenience then, it is assumed that the form of this bimodal, symmetric distribution should be a bimodal wrapped Gaussian function of the type defined in [Eq. \(4.1\)](#). This is a relatively convenient function for computer applications, and the parameters can be estimated directly from the Fourier coefficients of the measurements by the method of least squares described in [section 4](#). The resulting estimates are no less a valid realization as the MEM and MLM estimates.

The parameters resulting from the least squares fitting are presented in [Fig. 14](#) . [Figure 14a](#)  is a plot of the peak locations,  $\theta_{m1}$ ,  $\theta_{m2}$ , and [Fig. 14b](#)  is a plot of the angular width parameter  $\sigma$ . [Figure 14a](#)  also shows the Exact-NL curves for comparison. The peak locations of the symmetric double Gaussian are generally the same as those of the MEM ([Fig. 11](#) ) but the symmetric double Gaussian does not, however, show as clear a separation of the peaks as the MEM estimates for  $f/f_p < 2$ . The plot of the angular width parameter  $\sigma$  ([Fig. 14b](#) ) shows that it has a minimum at  $f_p$  and increases both for  $f/f_p < 1$  and for  $f/f_p > 1$ , but largely levels out for  $f/f_p > 1.7$ . The few points at  $f/f_p > 2$  with values of  $\sigma > 45^\circ$  corresponded to estimates in which the peak locations were closer together than the majority of neighboring points at those values of  $f/f_p$ —thus, the larger angular width makes up for the smaller angular separation of the peaks for those points.

The parameterization is established through two functions of the normalized frequency—one which models the angular separation of the peaks and another which models the shape of the angular width parameter. Clearly, there is a significant change in the behavior of the data at  $f_p$ , and to adequately account for this, a pair of functions for  $f/f_p < 1$  and another pair for  $f/f_p \geq 1$  are specified. There are any number of functions that can adequately describe the shape of the angular separation and angular width respectively; but this number is substantially reduced if the functions are also required to give a distribution that adequately describes the spreading parameters  $\sigma_1(f)$  and  $\sigma_2(f)$ .

The functions selected, based on curve fits, are as follows:

$$\Delta\theta = \exp\left[5.453 - 2.750\left(\frac{f}{f_p}\right)\right] \quad \text{for } f \geq f_p, \quad (6.4)$$

where  $\Delta\theta$  is the angular separation,  $\theta_{m2} - \theta_{m1}$ , of the peaks, and

$$\sigma = 11.38 + 5.357\left(\frac{f}{f_p}\right)^{-7.929} \quad \text{for } f < f_p$$

$$\sigma = 32.13 - 15.39\left(\frac{f}{f_p}\right)^{-2} \quad \text{for } f \geq f_p. \quad (6.5)$$

Thus, the angular separation is nonzero at all frequencies but set equal to the fixed value of 14.93 degrees for  $f < f_p$ .

Functions (6.4) and (6.5) together with Eq. (4.1) constitute the symmetric double Gaussian distribution. In the application of this parameterization the peaks are assumed to be at the same but opposite angles from the mean wave direction. The distribution parameters and the curves resulting from the parameterization are plotted in Fig. 15. Figure 15a is the plot of the angular separation of the peaks,  $\Delta\theta$ ; Fig. 15b is the Gaussian angular width parameter  $\sigma$ ; Fig. 15c is the circular rms  $\sigma_1$ ; and Fig. 15d is the directional spreading factor  $\sigma_2$ .

The shape of the symmetric double Gaussian with this parameterization is given in the shaded image plot in Fig. 16 and the frequency slices in Fig. 17. The frequency scale is  $f/f_p$  and the amplitudes have been normalized to one in both plots. The figures demonstrate clearly how the distribution is unimodal at low frequency and bimodal at higher frequencies having a shape rather like a tuning fork (Fig. 16). While the model is made up of two Gaussian components, the plots show that the distribution does not become bimodal in shape until  $f/f_p > 2$ . This is more consistent with the measured distributions when they are estimated from the MLM procedure rather than the MEM distribution, in which the bimodality becomes apparent at lower values of  $f/f_p$ , and it is consistent with the observations of Young et al. (1995).

## 7. Discussion

The Maui data suggest that fetch-limited sea states have bimodal directional distributions, but how important is it that this bimodality is included in calculations for practical purposes? To investigate this, a model fetch-limited sea state is constructed for a fetch of 200 km and a wind speed of 10 m s<sup>-1</sup>. The omnidirectional spectrum is modeled with a JONSWAP spectrum, and a frequency–direction spectrum is computed, each for the Hasselmann, Donelan–Banner, and symmetric double Gaussian directional distributions. The resulting distributions are plotted in polar form in Fig. 18. Figure 18a is a plot of the direction spectrum for each distribution type. The direction spectrum is calculated by integrating the frequency–direction spectrum over frequency. The radius at each angle is the spectral level (in m<sup>2</sup> deg<sup>-1</sup>). The figure shows that the overall directional distribution of energy of the symmetric double Gaussian remains unimodal; the more energetic components in the region of the peak of the spectrum therefore dominate the higher frequency, bimodal components.

Figure 18b is a polar plot of the directional distribution at  $f = 0.3$  Hz ( $\approx 3f_p$ ) for each of the three spectra. The radius at each angle is the spectral level (in units of m<sup>2</sup> Hz<sup>-1</sup> deg<sup>-1</sup>). As expected, this plot shows that at the higher frequencies the bimodality is significant.

Banner and Young (1994) conclude that the bimodality is a robust feature of predictions made using the full solution to the nonlinear wave–wave interaction source term in the spectral energy balance equation for wave growth. For computational efficiency, operational numerical wave models employ various approximations to the source terms. In 1G models the nonlinear wave–wave interaction source term is not considered; in 2G models the nonlinear source term is considered through a parameterization of the nonlinear spectral energy transfer and by constraining the spectral shape; and in 3G models the nonlinear interactions are approximated with a parameterization. Clearly, the 1G and 2G models, which assume a unimodal parameterization for the directional spreading, will not predict directional bimodality at  $f/f_p > 1$ . It is, however, not clear how well the 3G models will predict directional bimodality; but the results in Young et al. (1987) casts some doubt on this, particularly their Fig. 5, which shows differences in the directional spectra derived from the Exact-NL model and the 3G-WAM models. The Exact-NL spectrum shows bimodality, but the 3G-WAM spectrum does not.

Figure 18 shows that the prediction of bimodality is not likely to be significant within the active sea state. Thus,



engineering calculations of, say, the forces acting on a vertical pile in a sea state are unlikely to be compromised by assuming the directional distribution is unimodal. On the other hand, one can speculate that due to dispersion the bimodality may become more significant in the prediction of swell at a location some distance from the source and at relatively large angles from the direction of the wind field of the source. At such a location, the swell could be larger than predicted by current numerical models. Even at a location directly in line with the wind field of the source, it might be expected that, again due to dispersion, the energy of the swell might attenuate more quickly with time than predicted by current numerical models.

## 8. Conclusions

The integrated properties of the moments of the Maui directional distribution, and in particular the circular rms spreading and the directional spreading factor, are consistent with previously published results of [Hasselmann et al. \(1980\)](#) and [Donelan et al. \(1985\)](#), but their values are closer to those of the [Donelan et al. \(1985\)](#) distribution, which has a narrower spreading than that published in [Hasselmann et al. \(1980\)](#).

However, unlike the earlier results associated with a unimodal directional distribution at all frequencies, the Maui data provide convincing evidence for the presence of bimodal directional distributions at frequencies higher than the peak frequency. This supports the work of [Young et al. \(1995\)](#), who observed the same phenomenon but with observed bimodality occurring for  $f/f_p > 2$ . The Young et al. data were recorded in Lake George, a 2-m-deep lake in Australia. The Maui data were recorded in an open ocean location, where the water depth is 110 m, and over a large range of wind and wave conditions with wind speeds to  $20 \text{ m s}^{-1}$  and significant wave heights to 4.1 m. The bimodality remained a dominant feature of all of these conditions; thus the observations of the effect are extended to open ocean scales by the Maui data.

The results support the conclusion that nonlinear wave–wave interactions are responsible for the bimodality. No clear dependency of any of the directional parameters on wave age could be identified in the Maui data. Therefore, any contribution to the bimodality by the Phillip turbulent pressure fluctuation wave growth mechanism must be weak.

The proposed symmetric double Gaussian parameterization for the Maui directional distributions reproduces the essential features of measured directional distributions, giving a consistent circular rms spreading and directional spreading factor over frequency, at the same time as reproducing the bimodality at higher frequencies and approximating the peak width of the two peaks in the high-frequency directional distribution. This parameterization is useful for evaluating the qualitative aspects of the directional spreading and is probably as good as previously proposed distributions for quantitative evaluation, but it is expected that datasets acquired with higher-resolution instrumentation, together with more extensive analyses of the data than has been possible in this study, will ultimately lead to a more precise parameterization.

The parameterization has shown that, because the bimodality occurs at higher frequency with lower spectral levels, the total directional distribution of energy of a sea state remains unimodal. It therefore seems likely that, unless there is a particular application that has a strong frequency dependence, engineering calculations that make use of a simple unimodal description of the directional distribution are adequate. It is possible, however, that the existence of a bimodal directional distribution in real sea states may produce levels of swell at certain locations that are not well predicted by current numerical models.

## Acknowledgments

The wave directional data used in this study were provided by Shell, Todd Oil Services Ltd., New Plymouth, New Zealand. Their contribution is gratefully acknowledged. I would also like to thank Chris Shaw, George Forristall, and Paul Taylor for helpful comments and suggestions on a draft of this paper.

---

## REFERENCES

- Banner, M. L., 1990: Equilibrium spectra of wind waves. *J. Phys. Oceanogr.*, **20**, 966–984.
- , and I. R. Young, 1994: Modelling spectral dissipation in the evolution of wind waves. Part I: Assessment of existing model performance. *J. Phys. Oceanogr.*, **24**, 1550–1671.
- Benoit, M., 1993: Extensive comparison of directional wave analysis methods from gauge array data. *Proc. Second Int. Symp. on Ocean Wave Measurement and Analysis*, New Orleans, LA, ASCE, 740–754.
- Borgman, L. E., 1979: Directional wave spectra from wave sensors. *Ocean Wave Climate*, M. D. Earle and A. Matchoff, Eds., Plenum Press, 269–300.



- , and E. Yfantis, 1978: Measurement of directional wave spectra from fixed platforms. *Proc. MTS-IEEE Conf., The Ocean Challenge (OCEANS 78)*, Washington, D.C., MIS-IEEE, 634–638..
- Brissette, F. P., and I. K. Tsanis, 1994: Estimation of wave directional spectra from pitch–roll buoy data. *J. Waterway Port Coastal Ocean Eng.*, **120**, 93–115..
- Donelan, M. A., J. Hamilton, and W. H. Hui, 1985: Directional spectra of wind-generated waves. *Philos. Trans. Roy. Soc. London.*, **A315**, 509–562..
- Ewans, K. C., and A. C. Kibblewhite, 1990: An examination of fetch-limited wave growth off the west coast of New Zealand by a comparison with the JONSWAP results. *J. Phys. Oceanogr.*, **20**, 1278–1296..
- , and —, 1992: Spectral features of the New Zealand deep-water ocean wave climate. *N. Z. J. Mar. Freshwater Res.*, **26**, 323–338..
- Forristall, G. Z., and K. C. Ewans, 1998: Worldwide measurements of directional wave spreading. *J. Atmos. Oceanic Technol.*, **15**, 440–469..
- Haring, R. E., and J. C. Heideman, 1980: Gulf of Mexico rare wave return periods. *J. Petr. Technol.*, 35–47..
- Hasselmann, D. E., M. Dunkel, and J. A. Ewing, 1980: Directional wave spectra observed during JONSWAP 1973. *J. Phys. Oceanogr.*, **10**, 1264–1280..
- Hasselmann, K., and Coauthors, 1973: Measurements of wind-wave growth and swell decay during the Joint North Sea Wave Project (JONSWAP). *Dtsch. Hydrogr. Z.*, **8** (Suppl. A), 5–95..
- Isobe, M., K. Kondo, and K. Horikawa, 1984: Extension of MLM for estimating directional wave spectrum. *Symp. Description and Modelling of Directional Seas*. Copenhagen, Denmark, DHI and MMI, 1–15..
- Krogstad, H. E., 1991: Reliability and resolution of directional wave spectra from heave, pitch, and roll data buoys. *Directional Ocean Wave Spectra*, R. C. Beal, Ed., The Johns Hopkins University Press, 66–71..
- Kuik, A. J., G. Ph. van Vledder, and L. H. Holthuisen, 1988: A method for the routine analysis of pitch-and-roll buoy wave data. *J. Phys. Oceanogr.*, **18**, 1020–1034..
- Long, R. B., 1980: The statistical evaluation of directional spectrum estimates derived from pitch/roll buoy data. *J. Phys. Oceanogr.*, **10**, 944–952..
- Longuet-Higgins, M. S., D. E. Cartwright, and N. D. Smith, 1963: Observations of the directional spectrum of sea waves using the motions of a floating buoy. *Ocean Wave Spectra; Proceedings of a Conference*, Prentice-Hall, 111–131..
- Lygre, A., and H. E. Krogstad, 1986: Maximum entropy estimation of the directional distribution in ocean wave spectra. *J. Phys. Oceanogr.*, **16**, 2052–2060..
- Mitsuyasu, H., and Coauthors, 1975: Observations of the directional spectrum of ocean waves using a cloverleaf buoy. *J. Phys. Oceanogr.*, **5**, 750–760..
- Nwogu, O. U., E. P. D. Mansard, M. D. Miles, and M. Isaacson, 1987: Estimation of directional wave spectra by the maximum entropy method. *Proc. Wave Analysis and Generation in Laboratory Basins*, Lausanne, Switzerland, IAHR, 363–376..
- Welch, P. D., 1967: The use of the fast Fourier transform for the estimation of power spectra: A method based on time averaging over short modified periodograms. *IEEE Trans. Audio Electroacoust.*, **AU-15**, 70–73..
- Young, I. R., 1994: On the measurement of directional wave spectra. *Appl. Ocean Res.*, **16**, 283–294..
- , L. A. Verhagen, and M. L. Banner, 1995: A note on the bimodal directional spreading of fetch-limited wind waves. *J. Geophys. Res.*, **100** (C1), 773–778..

---

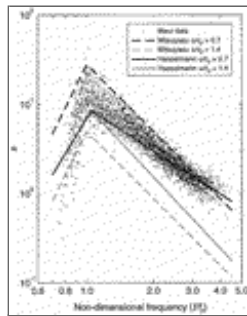
## Figures





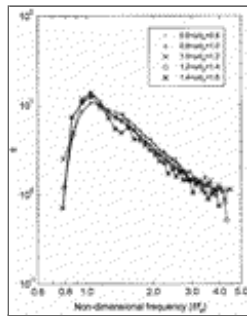
[Click on thumbnail for full-sized image.](#)

Fig. 1. The Greater Cook Strait Region of New Zealand. The WAVEC buoy was installed close to the Maui-A platform. The sector depicts a southeasterly fetch of 194 km from the measurement location.



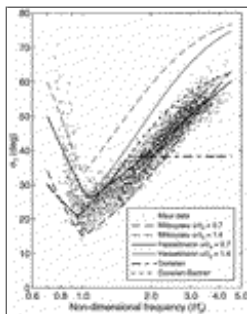
[Click on thumbnail for full-sized image.](#)

Fig. 2. The  $s$  parameter of the “cosine  $2s$ ” distribution, plotted as a function of  $ff_p$  for the Maui data and the Mitsuyasu and Hasselmann distributions.



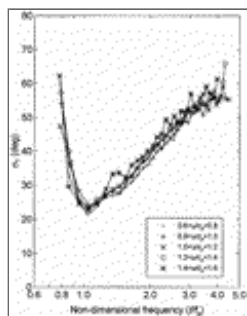
[Click on thumbnail for full-sized image.](#)

Fig. 3. Maui  $s$  parameter curves. Each curve is the average of  $s$  as a function of  $ff_p$  for the specified range of inverse wave age.



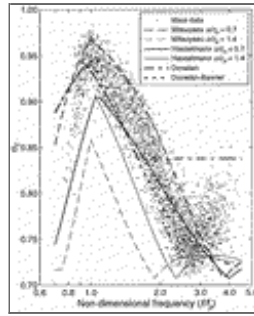
[Click on thumbnail for full-sized image.](#)

Fig. 4. Circular rms spreading  $\sigma_1$  plotted as a function of  $ff_p$  for the Maui data and the Mitsuyasu, Hasselmann, Donelan, and Donelan–Banner distributions.



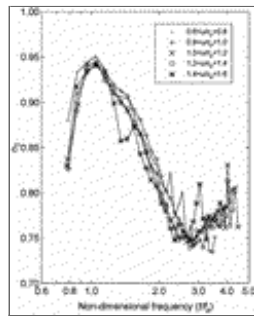
[Click on thumbnail for full-sized image.](#)

Fig. 5. Maui  $\sigma_1$  curves. Each curve is the average of  $\sigma_1$  as a function of  $f/f_p$  for the specified range of wave age.



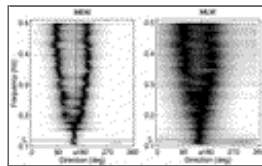
[Click on thumbnail for full-sized image.](#)

Fig. 6. Directional spreading factor  $\sigma_2$  plotted as a function of  $f/f_p$  for the Maui data and the Mitsuyasu, Hasselmann, Donelan, and Donelan–Banner distributions.



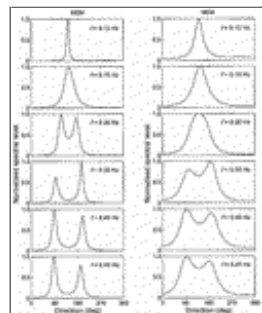
[Click on thumbnail for full-sized image.](#)

Fig. 7. Maui  $\sigma_2$  curves. Each curve is the average of  $\sigma_2$  as a function of  $f/f_p$  for the specified range of wave age.



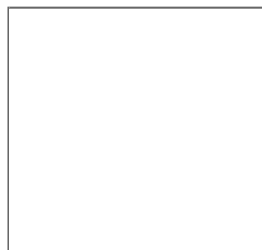
[Click on thumbnail for full-sized image.](#)

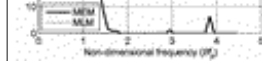
Fig. 8. Shaded image plot of the MEM and MLM estimates for one of the spectra ( $H_s = 3.8$  m,  $T_2 = 6.4$  s). Dark corresponds to high levels, light to low levels. The spectral levels at each frequency are normalized to have a maximum of one.



[Click on thumbnail for full-sized image.](#)

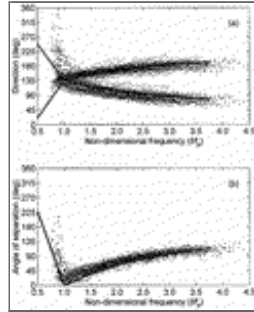
Fig. 9. Frequency slices through the shaded image plots in [Fig. 8](#).





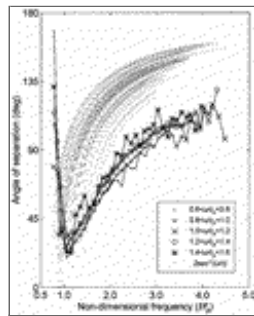
[Click on thumbnail for full-sized image.](#)

Fig. 10. The percentage of unimodal/symmetric MEM and MLM estimates plotted as a function of  $ff_p$ .



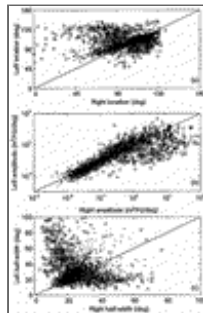
[Click on thumbnail for full-sized image.](#)

Fig. 11. Peak locations (a) and angular separation of peaks (b) of the pseudo-Voigt function components fitted to the MEM distributions.



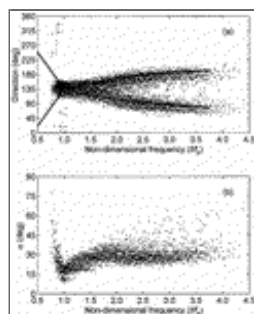
[Click on thumbnail for full-sized image.](#)

Fig. 12. Angular separation of peaks. Each curve is the average separation of the peaks of the pseudo-Voigt function fits to the MEM distributions, as a function of  $ff_p$ , for the specified range of inverse wave age. The points are the values of the peak separation defined by  $2 \text{sec}^{-1}(u/c)$  for the Maui data.



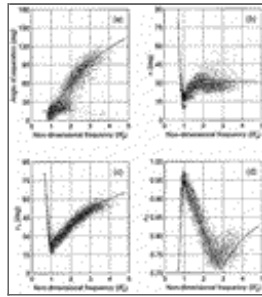
[Click on thumbnail for full-sized image.](#)

Fig. 13. Properties of the right (clockwise rotated from the mean direction) and left (anticlockwise rotated) components of the pseudo-Voigt function fits to the MEM distributions: (a) peak locations, (b) peak amplitudes, and (c) peak half-widths. Points with  $ff_p < 1.3$  are plotted as open circles.



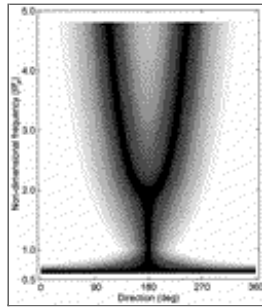
[Click on thumbnail for full-sized image.](#)

Fig. 14. Symmetric double Gaussian parameters, from fitting to the Maui data. (a) Peak locations, continuous lines are the locations of the Exact-NL data from [Young et al. \(1995\)](#), (b) spreading parameter  $\sigma$ .



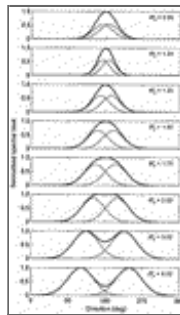
[Click on thumbnail for full-sized image.](#)

Fig. 15. Symmetric double Gaussian parameterization (continuous line) and Maui data (dots): (a) peak locations, (b) spreading parameter  $\sigma$ , (c) circular rms spreading  $\sigma_1$ , and (d) spreading factor  $\sigma_2$ .



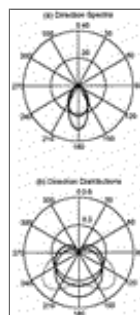
[Click on thumbnail for full-sized image.](#)

Fig. 16. Shaded image plot of the symmetric double Gaussian spectrum. Dark corresponds to high levels, light to low levels. The spectral levels are normalized to have a maximum of one.



[Click on thumbnail for full-sized image.](#)

Fig. 17. Frequency slices through the symmetric double Gaussian spectrum presented in [Fig. 15](#). Thin lines are the separate Gaussian components.



[Click on thumbnail for full-sized image.](#)

Fig. 18. Polar plots of (a) the direction spectrum and (b) the directional distribution at 0.30 Hz for a fetch-limited sea state with a fetch of 200 km and a wind speed of  $10 \text{ m s}^{-1}$ . Thin lines: the symmetric double Gaussian distribution; medium thick lines: the Donelan distribution; and thick lines: the Hasselmann distribution.

*Corresponding author address:* Dr. Kevin C. Ewans, Shell International Exploration and Production B.V., Volmerlaan 8, P.O. Box 60, 2280 AB Rijswijk, the Netherlands.

E-mail: [k.ewans@siep.shell.com](mailto:k.ewans@siep.shell.com)

top ▲



© 2008 American Meteorological Society [Privacy Policy and Disclaimer](#)  
Headquarters: 45 Beacon Street Boston, MA 02108-3693  
DC Office: 1120 G Street, NW, Suite 800 Washington DC, 20005-3826  
[amsinfo@ametsoc.org](mailto:amsinfo@ametsoc.org) Phone: 617-227-2425 Fax: 617-742-8718  
[Allen Press, Inc.](#) assists in the online publication of *AMS* journals.